

RSC Advances



This is an *Accepted Manuscript*, which has been through the Royal Society of Chemistry peer review process and has been accepted for publication.

Accepted Manuscripts are published online shortly after acceptance, before technical editing, formatting and proof reading. Using this free service, authors can make their results available to the community, in citable form, before we publish the edited article. This *Accepted Manuscript* will be replaced by the edited, formatted and paginated article as soon as this is available.

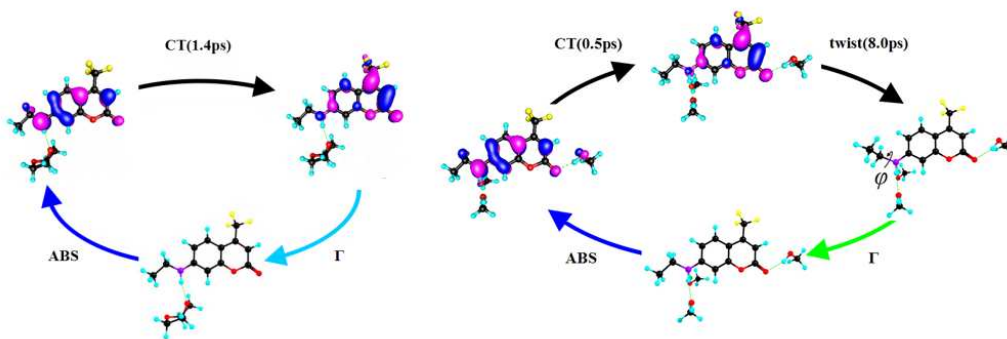
You can find more information about *Accepted Manuscripts* in the [Information for Authors](#).

Please note that technical editing may introduce minor changes to the text and/or graphics, which may alter content. The journal's standard [Terms & Conditions](#) and the [Ethical guidelines](#) still apply. In no event shall the Royal Society of Chemistry be held responsible for any errors or omissions in this *Accepted Manuscript* or any consequences arising from the use of any information it contains.

Graphical Abstract

Different Mechanisms of Ultrafast Excited State Deactivation of
Coumarin 500 in Dioxane and Methanol Solvents: Experimental and
Theoretical Study

Lin Cong, Han Yin, Ying Shi*, Mingxing Jin, Dajun Ding



The effect of hydrogen bond on the intermolecular photoinduced ICT and TICT processes for Coumarin 500 have been demonstrated, and a reliable mechanism has been revealed on the unusual properties of C500 in Dioxane and Methanol.

**Different Mechanisms of Ultrafast Excited State
Deactivation of Coumarin 500 in Dioxane and Methanol
Solvents: Experimental and Theoretical Study**

Lin Cong, Hang Yin, Ying Shi*, Mingxing Jin, Dajun Ding

Institute of Atomic and Molecular Physics, Jilin University, Changchun

130012, China

E-mail address: shi_ying@jlu.edu.cn (Ying Shi)

Tel: +86-431-85168817 Fax: +86-431-85168816

Abstract

Solute-solvent intermolecular photoinduced intramolecular charge transfer (ICT) and twisted intramolecular charge transfer (TICT) states are proposed to account for the unusual properties of coumarin 500 (C500) in 1,4-dioxane (Diox) and methanol (MeOH) solvents. Our femtosecond transient absorption experiment on C500 shows that in Diox, there exists a single exponential component with time constant $\tau_1 \sim 1.4$ ps, however in MeOH two exponential components with lifetimes $\tau_1 \sim 0.5$ ps and $\tau_2 \sim 8.0$ ps are observed. DFT and TDDFT methods were used to optimize geometries of complexes C500-Diox and C500-(MeOH)₃ in the ground and excited states, respectively. It shows that the rapid decay time could be due to ICT and ICT→TICT could be responsible for the slow decay time. Strengthening of hydrogen bond N-H...O-H and the weakening of hydrogen bond N...H-O in the excited state of C500-(MeOH)₃ complex could facilitate the process of ICT from 7-NHEt group to CF₃ group and induce the formation of TICT state in hydrogen bonding MeOH. Together, the experimental and theoretical results reveal that C500 exhibits unusual deactivation mechanisms in Diox and MeOH solvents.

Keywords

Hydrogen bond; Excited state; Transient absorption spectroscopy;
TDDFT; ICT; TICT

1. Introduction

The coumarin dyes, generally known as the derivatives of 1,2-benzopyrone, were an important class of well-known laser dyes for the blue-green region.¹⁻⁷ The 7-aminocoumarin dyes were special among the coumarin dyes, due to their excellent laser activity and great applicability to study many processes of physicochemistry.¹⁻⁷ The 7-aminocoumarin dyes often had very strong fluorescence with their fluorescence quantum yields approaching unity.¹⁻¹⁰ In these compounds the deexcitation of fluorescence occurred to some extent via internal conversion (IC) and negligible intersystem crossing (ISC).⁸⁻¹⁰ During photoexcitation, most 7-aminocoumarin dyes showed large changes in dipole moment when going from ground state to their electronic excited states.¹⁻¹⁰ All 7-aminocoumarin dyes exhibited large solvatochromic shifts in their absorbance and fluorescence spectra.⁸⁻¹⁷ The remarkable solvatochromic properties of these dyes can be attributed to intramolecular charge transfer (ICT) from the electron donor amino group to the electron acceptor carbonyl group.^{18,19}

Coumarin 500 (C500, Figure 1A) was a typical 7-aminocoumarin dye that was widely used as fluorescence probe doping in varied systems and have been researched by many steady-state, transient-state spectroscopic methods.²⁰⁻³⁸ Few years back, Nad et al. had studied the photophysical properties of C500 in a series of solvents, from nonpolar

solvents to polar solvents and alcoholic solvents. They measured the optical absorption and fluorescence spectra of C500 in different solvents indicated that C500 exhibited unusual spectral behaviors in nonpolar solvents. Importantly, the Stokes shifts and fluorescence lifetimes for C500 were found to be unusually high, also the fluorescence quantum yields and radiative decay rate constants for C500 were seen to be unusually low in alcoholic solvents, which indicated that the solute-solvent hydrogen bond had a strong influence on the photophysical properties of C500.³⁹ Recently, the rotational reorientation dynamics of C500 in methanol, dimethyl formamide, and dimethyl sulfoxide had been investigated by femtosecond time-resolved stimulated emission pumping fluorescence depletion spectroscopy using a 400 nm pump pulse and a 490 nm probe pulse. Zhou et al. had proposed that the rapid anisotropy decays may be associated with solute-solvent intermolecular hydrogen bond.⁴⁰ In fact, Zhao et al. demonstrated that electronically excited state early time hydrogen bonding dynamics of coumarin 102 was closely related to many important phenomena such as internal conversion (IC), intermolecular charge transfer and fluorescence quenching in hydrogen bonding solvents.⁴¹⁻⁴⁸ However, the influence of solute-solvent intermolecular hydrogen bonding on the unusual behavior of C500 has not been investigated so far, in order to obtain complete photochemical information, it was necessary to explore the spectral properties of the

broadband transient absorption of C500 in hydrogen bonding solvent system.

C500 may accept hydrogen bonds at the nitrogen lone pair and the carbonyl group from hydrogen bond donating solvents, and C500 may also establish such bonds with hydrogen bond accepting solvents from the H-atom on the amino group, as shown in Figure 2.³¹ The 1,4-dioxane (Diox, Figure 1B) and methanol (MeOH) have similar polarity, but capable of forming different types of hydrogen bonds is different, where MeOH has hydrogen bond acceptor and hydrogen donor properties, while Diox only has hydrogen bond acceptor property.³¹ In this work, we have presented here a femtosecond transient absorption study on the excited state dynamics of C500 in Diox and MeOH solvents. In addition, we have also employed the quantum chemical calculation to simulate the two different environments. The results from the above experiments and calculations have been used to understand the different ultrafast excited state deactivation mechanisms of C500 in two different hydrogen bonding systems.

2. Methods

2.1. Experimental Methods

Ultrapure grade C500 was purchased from Exciton (USA) and used without further purification. Diox and MeOH were spectrum pure quality reagents. The concentration of C500 in Diox and MeOH was 50 μM .

The steady-state absorption and fluorescence spectra were measured by Cary 500 UV-Vis-NIR Spectrophotometer and Cary Eclipse Fluorescence Spectrophotometer (Varian), respectively. The ultrafast dynamics of C500 in Diox and MeOH were measured using transient absorption technique. The details of the experimental setup have been described elsewhere.⁴⁹ Briefly, the system produced fundamental laser by a Ti:sapphire pulse pumped oscillation and a regenerative amplifier (Spectral Physics) both operating at 1kHz repetition rate. The output wavelength of the system was 800 nm where the full width at half maximum (FWHM) was 90 fs and the output power was approximately 600 mW. The fundamental laser was separated into two beams in the ratio 9:1.

The more intense beam was used for generating the second harmonic ($\lambda_{\text{exc}} = 400 \text{ nm}$) of the fundamental laser by a 0.5 mm BBO ($\beta\text{-BaB}_2\text{O}_4$, Fujian Castech Crystals Inc. China), which was applied to be pump laser for exciting samples. The energy per pump pulse at the sample was about $2\mu\text{J}$. The other beam passed through a controlled delay line and then focused into a sapphire plate to generate a sub-picosecond white-light supercontinuum, which served as the probe laser. Two laser beams were incident on the sample in a 0.5 cm quartz cuvette at a small angle ($\theta \leq 5^\circ$). The fused quartz sample cell was placed in the beam path where the beam diameter was 2 mm. The sample cuvette was stirred using a magnetic

stirrer bar during the data acquisition. The FWHM of the correlation function of the two beams was 153 fs and the intrinsic temporal resolution was 7 fs. Intrinsic resolution of fiber optics coupled multichannel spectrometer with CMOS sensor was 1.5 nm.

The transient absorption spectra were measured at room temperature between 420-650 nm and were corrected for group velocity dispersion of the white light continuum.

2.2. Computational Methods

Ground state geometric structures and energies of both isolated monomers and solute-solvent hydrogen-bonded complexes were calculated using the density functional theory (DFT) method with the generalized gradient approximation (GGA) for exchange correlation potential BP86. Vertical singlet-state excitation energy calculations and excited state geometry optimizations were performed using the time-dependent density functional (TDDFT) method and the same exchange correlation potential for excited state.⁵⁰⁻⁶¹ The resolution of the identity (RI) approximation was also used to improve the efficiency without sacrificing the accuracy of the results.⁵¹⁻⁵³ Previous electronic structure computations were performed with the Turbomole program suite.⁵⁰⁻⁵⁵ The correction for energy level order of hydrogen-bonded complexes was calculated using the other exchange correlation potential CAM-B3LYP, which is performed with the Gaussian 09 program suite.⁶²

The triple- ζ valence with one set of polarization functions (TZVP) was chosen as basis sets throughout.⁵⁴

3. Results and Discussion

3.1. Steady-State Spectra and Electronic Excitation Energy Calculations

The normalized steady-state absorption and fluorescence spectra of C500 in Diox and MeOH solvents are shown in Figure 3. Absorption spectrum of C500 in Diox reveals an absorption band centered at 376 nm. In MeOH, the broad absorption band is centered at 392 nm, which is in good agreement with the results of Jain and Nad.^{31,39}

C500 has three positions to form hydrogen bonds through carbonyl oxygen: C=O...H-O (Type A), amino hydrogen: N-H...O (Type B) and amino nitrogen: N...H-O (Type C) shown in Figure 2, where Diox only may form hydrogen bond in position B and MeOH may form three kinds of hydrogen bonds in all positions.^{31,63} So we focused on the solute-solvent hydrogen-bonded complexes C500-Diox and C500-(MeOH)₃ in gas phase to simulate the environments of C500 in Diox and MeOH solvents, respectively. The electronic excitation energies and the corresponding oscillator strengths obtained from TDDFT calculations on the complexes C500-Diox and C500-(MeOH)₃ in the low-lying electronic excited states are listed in Table 1. One can see that the oscillator strength corresponding to the S₁ state of complex

C500-Diox is the largest, which means the absorption maximum of C500-Diox is located in the S_1 state, and the calculated absorption spectrum of C500-Diox is centered at 427 nm. As with complex C500-(MeOH)₃, the S_2 state has the highest oscillator strength, hence the theoretical value of C500-(MeOH)₃ absorption maximum is 420 nm, also fitted with 392 nm measured in experiment. By frontier molecular orbital calculation (Table 1), both the S_1 state of C500-Diox and the S_2 state of C500-(MeOH)₃ are ICT states and the calculated S_1 state of complex C500-(MeOH)₃ is a dark state, which is corresponding to an intermolecular CT state (see Section 3.3) based on Ref⁴⁰.

The fluorescence maxima in MeOH (500 nm) is significantly red-shifted compared to 463 nm in Diox (Figure 1), which is in line with Ref³⁹. The Stokes shift in MeOH is 108 nm which is much larger than in Diox (74 nm). The most plausible explanation for this large Stokes shift is ICT from electron-donor 7-NHEt group to the electron-acceptor CF₃.³⁹

3.2. Transient Absorption Measurement

Transient absorption spectra of C500 in Diox and MeOH solvents are measured with the excitation at 400 nm. The early spectral evolution of C500 in Diox (Figure 4A) from 0 to 8.8 ps shows a strong positive band located around 430 nm and a broad negative band in the 440-650 nm region. A comparison of the spectra of the transients with the steady state absorption and fluorescence spectra of C500 in Diox and MeOH

identifies the negative signal as stimulated emission and positive signal as excited state absorption. And likewise, Figure 4B shows the transient absorption spectrum of C500 in MeOH from 0 to 11.8 ps where the excited state absorption at 425 nm is slightly blue-shifted and the stimulated emission peak from 466-523 nm is red-shifted compared to that in Diox.

Kinetic traces for selected probe wavelengths at 426 and 480 nm of transient absorption for C500 in Diox solvent are shown in Figure 5A. The absorption band at 426 nm and the gain band at 480 nm grow rapidly within 1-2 ps. It shows that most of C500 molecule located in the ground state is very rapidly converted in to a transient ICT state.

The kinetic curves for C500 in MeOH at 426 nm and 480 nm (Figure 5B) also show a rapid increase within 1 ps which indicates conversion of ground state to the transient ICT state similar to what is observed in Diox. However, Unlike in Diox, the rapid absorption change at 426 nm and 480 nm is also followed by (at $\tau > 1.4$ ps) a large shift in the stimulated emission maximum from 466 to 523 nm. This implies the existence of another intermediate state, which results in the broadening and lowering in energy of the gain band from 440-600 nm to 440-650nm. From our calculations on the excited state of C500 (reported in the next section), we attributed this emerging second intermediate state to the

twisting of 7-NHEt group in C500 and the red-shifted fluorescence emission to twisted intramolecular charge transfer (TICT) state of C500.

A global analysis was used where sets of kinetic curves were fit simultaneously using exponential components with common lifetimes (Table 2). We attributed the monoexponential component with lifetime $\tau_1 \sim 1.4$ ps to ICT. The kinetic curves for C500 in MeOH were fitted to two exponentials with lifetimes $\tau_1 \sim 0.5$ ps and $\tau_2 \sim 8.0$ ps. The biexponential model provided better fits to the experimental data, indicating that the contribution from the second component cannot be ignored. The two exponential components in MeOH were associated with ICT and ICT \rightarrow TICT conversion as has been reported for coumarin 481 in Ref⁶⁴. In addition, our results are consistent with the suggestion that hydrogen bond facilitates charge transfer mechanisms as suggested by Fiebig.⁶⁵

To obtain further insight the different ultrafast excited state deactivation schemes for C500 in Diox and MeOH solvents, we plotted 3D images (Figure 6) of transient absorption for C500 in Diox and MeOH solvents as a function of wavelength and time delay after excitation. We attributed the red and blue regions to transient absorption and stimulated emission, respectively. ICT absorption and ICT emission were observed in both solvents (Figure 6), whereas TICT was observed only in MeOH. The large spectral differences could be attributed to differences in hydrogen bonding interactions between C500 and Diox and MeOH.

3.3. Quantum Chemical Calculation

In order to test the validity of the above conclusion, we obtained optimized geometric structures of the hydrogen-bonded complexes C500-Diox and C500-(MeOH)₃ in ground state (Figure 7). In order to obtain deeper insight into the ICT process, we plotted the frontier molecular orbitals (FMOs) of the two complexes (Figure 8). It can be clearly seen that both complexes have larger electron density on the 7-NHEt group and smaller electron density on the CF₃ group in the HOMO than that in the LUMO. From the results listed in Table 1, it can be seen that both the S₁ state of complex C500-Diox and the S₂ state of complex C500-(MeOH)₃ corresponds to the orbital transition from HOMO to LUMO and that ICT occurs from 7-NHEt group to CF₃ group in C500 (Figure 8). Similarly, the intermolecular CT state, that is, the S₁ state of complex C500-(MeOH)₃ corresponds to the orbital transition from HOMO-1 to LUMO and that intermolecular CT occurs between C500 and MeOH. It is worth noting that the S₁ and S₂ state of complex C500-(MeOH)₃ corresponds to the orbital transition from HOMO-1 to LUMO and HOMO to LUMO, respectively, but the energy of S₁ state (511 nm) is lower than that of S₂ state (420 nm). On the other hand, the intermolecular CT state is a non-fluorescent state, which is not responsible for fluorescence quenching in the complex. So it appears that the energy of the intermolecular CT state in the complex may have been

underestimated by the BP86 density functional. In order to obtain better estimates of charge transfer character and energies, we used the long-range corrected density functional and recalculated electronic excitation energies and FMOs for complex C500-(MeOH)₃ by CAM-B3LYP (Table 1).^{61,66,67} Through a comparative analysis of FMOs, we found that the new S₁ state was ICT state, which corresponded to the previously calculated S₂ state of complex C500-(MeOH)₃, whereas the new S₂ state was intermolecular CT state, which corresponded to the previously calculated S₁ state of complex C500-(MeOH)₃. In fact, the energy of ICT state is lower than that of intermolecular CT state after long-range corrected resulting that both ICT state of C500-(MeOH)₃ and ICT state of monomer C500 are located in the first electronically excited state (S₁).

From the optimized geometries obtained from DFT and TDDFT calculations using the BP86 functional, we obtained the lengths of intermolecular hydrogen bonds in the ground state and ICT state for complexes C500-Diox and C500-(MeOH)₃ (Table 3). As with C500-Diox, Diox only can form hydrogen bond with C500 in position B. The length of hydrogen bond N-H...O (Type B) was calculated to be 1.999 and 1.902 Å in ground state and ICT state, respectively. The hydrogen bond of type B is strengthened slightly observed in the ICT state. For complex C500-(MeOH)₃, MeOH can form three kinds of hydrogen bonds in all

positions, where the length of hydrogen bond C=O...H-O (Type A) was calculated to be 1.905 and 1.852 Å in ground state and ICT state, respectively. And the intermolecular hydrogen bond N-H...O-H (Type B), which is formed between 7-NHEt hydrogen atom and hydroxyl oxygen atom and reside out of the plane of coumarin, was calculated to be 1.930 and 1.848 Å in ground state and ICT state, respectively. We can find that the hydrogen bonds of types A and B are strengthened in the ICT state. The intermolecular hydrogen bond N...H-O (Type C), combined between 7-NHEt nitrogen atom and hydroxyl hydrogen atom and nearly perpendicular to the plane of coumarin. The length of hydrogen bond type C was calculated to be 2.028 Å in ground state and it is the longest by the weakest of the three different kinds of intermolecular hydrogen bonds by calculation. Also the hydrogen bond of type C was calculated to be 2.404 Å in the ICT state and much weaker than that in ground state. As shown in Figure 7, the C500-Diox is nearly planar whereas the C500-(MeOH)₃ is not, herein it should be noticed that the hydrogen bonds B and C play a very important role in changing the conformation of coumarin plane. A possible explanation for change in the conformation is that upon optical excitation of C500, as the electron density on the 7-NHEt group decreases, the hydrogen bond of type B strengthens and hydrogen bond of type C weakens inducing the twisting of 7-NHEt, resulting in the formation of TICT state. We found out the TICT state by calculation (Figure 9), and

the calculated dihedral angle between the plane of coumarin and the plane of 7-NHEt were calculated to be 4.2°, 2.8° and 78.4° in ground, ICT and TICT state, respectively. One can see that in the structure of complex C500-(MeOH)₃ in ICT state, the 7-NHEt group is almost in the plane of coumarin, whereas in the TICT state, the 7-NHEt group undergoes a remarkable 75.6° twist and is nearly perpendicular to the plane of coumarin in TICT state (Figure 9). These results provide clear evidence for ICT from 7-NHEt group to CF₃ group and the existence of TICT state in MeOH.

3.4. Excited State Deactivation Mechanism

On the basis of the steady-state as well as transient absorption results, the different deactivation mechanisms for the excited state of the C500 in Diox and MeOH are shown in Figure 10.

In Diox and MeOH solvents, where the hydrogen bonding effects are different, dramatic effects are observed in the fluorescence and transient absorption spectra. When the C500 is excited in Diox, it returns to the ground state emitting fluorescence with maximum at 463 nm as a result of efficient ICT with a life time of $\tau_1 \sim 1.4$ ps. Upon photoexcitation of the dye in MeOH, C500 very rapidly converts to ICT state with a faster lifetime $\tau_1 \sim 0.5$ ps. The results from our quantum chemical calculations show that, the dihedral angle between the plane of coumarin and the plane of 7-NHEt group changes from 4.2° (HOMO) to

2.8° (ICT). Once in the ICT state, the electron density on the 7-NHEt group decreases, concomitantly with the increase in strength of hydrogen bond B and weakening of hydrogen bond C. This leads to a rotation of the 7-NHEt group which changes the torsional angle from 2.8° to 78.4° leaving the molecule in the TICT state characterized by the $\tau_2 \sim 8.0$ ps component. Finally, C500 in TICT returns to the ground state with a fluorescence emission maximum at 499 nm.

4. Conclusions

We have described here the excited state dynamics of C500 in Diox and MeOH solvents through transient absorption spectroscopy. It was found that the dynamics of C500 in Diox exhibited an absorption band at 420-440 nm, gain band at 440-600 nm with a single exponential time constant of $\tau_1 \sim 1.4$ ps. However, in MeOH, an absorption band was observed at 420-440 nm, and a gain band at 450-650 nm with double exponential time constants of $\tau_1 \sim 0.5$ ps and $\tau_2 \sim 8.0$ ps. The short decay time may be associated with ICT and the long decay time may be related to the ICT→TICT conversion. We have also presented computational results at the TD-BP86/TZVP and CAM-B3LYP/TZVP level including the optimized geometric structures, energies and MOs of solute-solvent hydrogen-bonded complexes C500-Diox and C500-(MeOH)₃ in the ground and excited states. Our results from TDDFT calculations show that, as for C500-Diox, the hydrogen bond of type B is strengthened

slightly observed in the ICT state. As with C500-(MeOH)₃, while the hydrogen bonds of types A and B are strengthened, the hydrogen bond type C is weakened, resulting in the rotation of 7-NHEt group which is nearly planar (4.2°) geometry in the ground state to nearly perpendicular (78.4°) in the TICT state. Most importantly, we have shown that the change of hydrogen bonding may facilitate ICT from 7-NHEt group to CF₃ group, which induces the formation of TICT state in MeOH. Thus this study provides deeper mechanistic insights into the photochemistry of C500 in different hydrogen bonded solvents.

Acknowledgements

This work is supported by the National Basic Research Program of China (973 Program, Grant No. 2013CB922200), the National Natural Science Foundation of China (Grant No. 11174106, 10974069) and the Natural Science Foundation of Jilin Province of China (Grant No. 201115018).

Notes and References

1. R. L. Atkins and D. E. Bliss, *J. Org. Chem.*, 1978, **43**, 1975-1980.
2. A. N. Fletcher and D. E. Bliss, *Appl. Phys.*, 1978, **16**, 289-295.
3. J. A. Halstead and R. R. Reeves, *Optics. Comm.*, 1978, **27**, 273-276.
4. A. N. Fletcher, *Appl. Phys.*, 1977, **14**, 295-302.
5. H. Y. Bai, J. H. Qian, H. Y. Tian, W. W. Pan, L. Y. Zhang and W. B. Zhang, *Dyes Pigments*, 2014, **103**, 1-8.
6. K. Dobek, J. Karolczak and J. Kubicki, *Dyes Pigments*, 2014, **100**, 222-231.
7. K. Khemakhem, H. Ammar, S. Abid, R. El Gharbi and S. Fery-Forgues, *Dyes Pigments*, 2013, **99**, 594-598.
8. G. Jones II, W. R. Jackson and S. Konaktanaporn, *Opt. Commun.*, 1980, **33**, 315-320.
9. G. Jones II, W. R. Jackson and A. M. Halpem, *Chem. Phys. Lett.*, 1980, **72**, 391-395.
10. G. Jones II, W. R. Jackson, C. Choi and W. R. Bergmark, *J. Phys. Chem.*, 1985, **89**, 294-300.
11. M. Maroncelli and G. R. Fleming, *J. Chem. Phys.*, 1987, **86**, 6221-6239.
12. M. L. Horng, J. A. Gardecki, A. Papazyan and M. Maroncelli, *J. Phys. Chem.*, 1995, **99**, 17311-17337.

13. K. Tominaga and G. C. Walker, *J. Photochem. Photobiol. A*, 1995, **87**, 127-133.
14. M. Maroncelli, *J. Mol. Liq.*, 1993, **57**, 1-37.
15. J. A. Gardecki and M. Maroncelli, *J. Phys. Chem.*, 1999, **103**, 1187-1197.
16. C. F. Chapman and M. Maroncelli, *J. Phys. Chem.*, 1991, **95**, 9095-9114.
17. M. A. Kahlow, W. Jarzeba, T. J. Kang and P. F. Barbara, *J. Chem. Phys.*, 1989, **90**, 151-158.
18. P. K. McCarthy and G. J. Blanchard, *J. Phys. Chem.*, 1993, **97**, 12205-12209.
19. K. Rechthaler and G. Köhler, *Chem. Phys.*, 1994, **189**, 99-116.
20. H. Mesnil, M. C. Schanne-Klein and F. Hache, *Eur. Phys. J. D*, 1999, **5**, 447-452.
21. S. Uppili, K. J. Thomas, E. M. Crompton and V. Ramamurthy, *Langmuir*, 2000, **16**, 265-274.
22. K. Das, B. Jain and P. K. Gupta, *Chem. Phys. Lett.*, 2005, **410**, 160-164.
23. P. Majumder, R. Sarkar, A. K. Shaw, A. Chakraborty and S. K. Pal, *J. Colloid Interf. Sci.*, 2005, **290**, 462-474.
24. L. S. Rohwer and J. E. Martin, *J. Lumin.*, 2005, **115**, 77-90.

25. Y. Yang, G. D. Qian, D. L. Su, Z. Y. Wang and M. Q. Wang, *Chem. Phys. Lett.*, 2005, **402**, 389-394.
26. J. E. Martin and L. E. Shea-Rohwer, *J. Lumin.*, 2006, **121**, 573-587.
27. R. K. Mitra, S. S. Sinha and S. K. Pal, *Langmuir*, 2008, **24**, 49-56.
28. R. K. Mitra, S. S. Sinha, R. K. Verma and S. K. Pal, *J. Phys. Chem. B*, 2008, **112**, 12946-12953.
29. S. S. Narayanan, S. S. Sinha, R. Sarkar and S. K. Pal, *J. Phys. Chem. B*, 2008, **112**, 2859-2867.
30. S. S. Narayanan, S. S. Sinha, R. Sarkar and S. K. Pal, *Chem. Phys. Lett.*, 2008, **452**, 99-104.
31. K. Das, B. Jain and H. S. Patel, *J. Phys. Chem. A*, 2006, **110**, 1698-1704.
32. P. K. Verma, R. K. Mitra and S. K. Pal, *Langmuir*, 2009, **25**, 11336-11343.
33. P. K. Verma, R. Saha, R. K. Mitra and S. K. Pal, *Soft Matter*, 2010, **6**, 5971-5979.
34. S. Banerjee, P. K. Verma, R. K. Mitra, G. Basu and S. K. Pal, *J. Fluoresc.*, 2012, **22**, 753-769.
35. S. Rakshit, R. Saha, P. K. Verma and S. K. Pal, *Photochem. Photobiol.*, 2012, **88**, 851-859.
36. A. Das, A. Patra and R. K. Mitra, *J. Phys. Chem. B*, 2013, **117**, 3593-3602.

37. D. De, M. Sajjan, J. Narayanan, J. R. Bellare and A. Datta, *J. Phys. Chem. B*, 2013, **117**, 2106-2112.
38. A. Patra, T. Q. Luong, R. K. Mitra and M. Havenith, *Phys. Chem. Chem. Phys.*, 2013, **15**, 930-939.
39. S. Nad and H. Pal, *J. Phys. Chem. A*, 2003, **107**, 501-507.
40. P. W. Zhou, P. Song, J. Y. Liu, K. L. Han and G. Z. He, *Phys. Chem. Chem. Phys.*, 2009, **11**, 9440-9449.
41. K. L. Han and G. J. Zhao, *Wiley Online Library*, 2011.
42. G. J. Zhao and K. L. Han, *Acc. Chem. Res.*, 2012, **45**, 404-413.
43. C. Miao and Y. Shi, *J. Comput. Chem.*, 2011, **32**, 3058-3061.
44. G. J. Zhao and K. L. Han, *J. Phys. Chem. A*, 2009, **113**, 14329-14335.
45. G. J. Zhao and K. L. Han, *Biophys. J.*, 2008, **94**, 38-46.
46. G. J. Zhao and K. L. Han, *J. Comput. Chem.*, 2008, **29**, 2010-2017.
47. G. J. Zhao and K. L. Han, *Chem. Phys. Chem.*, 2008, **9**, 1842-1846.
48. G. J. Zhao and K. L. Han, *J. Phys. Chem. A*, 2007, **111**, 2469-2474.
49. A. P. Blokhin, M. F. Gelin, O. V. Buganov, V. A. Dubovskii, S. A. Tikhomirov and G. B. Tolstorozhev, *J. Appl. Spectrosc.*, 2003, **70**, 70-79.
50. F. Furche and R. Ahlrichs, *J. Chem. Phys.*, 2002, **117**, 7433-7447.
51. J. L. Whitten, *J. Chem. Phys.*, 1973, **58**, 4496-4501.
52. B. L. Dunlap, J. W. D. Conolly and J. R. Sabin, *J. Chem. Phys.*, 1979, **71**, 3396-3402.

53. O. Vahtras, J. E. Almlöf and M. W. Feyereisen, *Chem. Phys. Lett.*, 1993, **213**, 514-518.
54. A. Schafer, C. Huber and R. Ahlrichs, *J. Chem. Phys.*, 1994, **100**, 5829-5835.
55. R. Ahlrichs, M. Bar, H. Horn and C. Kolmel, *Chem. Phys. Lett.*, 1989, **162**, 165-169.
56. M. Sun, *J. Chem. Phys.*, 2006, **124**, 054903-054908.
57. M. Sun, Y. Ding and H. Xu, *J. Phys. Chem.*, 2007, **111**, 13266-13270.
58. P. Song, Y. Li, F. Ma, T. Pullerits and M. Sun, *J. Phys. Chem.*, 2013, **117**, 15879-15889.
59. M. T. Sun, Y. R. Fang, Z. L. Yang and H. X. Xu, *Phys. Chem. Chem. Phys.*, 2009, **11**, 9412-9419.
60. S. B. Cheng, P. Song, S. Q. Yang, H. M. Yin and K. L. Han, *Phys. Chem. Chem. Phys.*, 2010, **12**, 9068-9075.
61. P. W. Zhou, J. Y. Liu, S. Q. Yang, J. S. Chen, K. L. Han and G. Z. He, *Phys. Chem. Chem. Phys.*, 2012, **14**, 15191-15198.
62. M. J. Frisch, G. W. Trucks, H. B. Schlegel, G. E. Scuseria, M. A. Robb, J. R. Cheeseman, G. Scalmani, V. Barone, B. Mennucci, G. A. Petersson, H. Nakatsuji, M. Caricato, X. Li, H. P. Hratchian, A. F. Izmaylov, J. Bloino, G. Zheng, J. L. Sonnenberg, M. Hada, M. Ehara, K. Toyota, R. Fukuda, J. Hasegawa, M. Ishida, T. Nakajima, Y. Honda, O. Kitao, H. Nakai, T. Vreven, J. A. Jr. Montgomery, J. E. Peralta, F. Ogliaro, M.

Bearpark, J. J. Heyd, E. Brothers, K. N. Kudin, V. N. Staroverov, T. Keith, R. Kobayashi, J. Normand, K. Raghavachari, A. Rendell, J. C. Burant, S. S. Iyengar, J. Tomasi, M. Cossi, N. Rega, J. M. Millam, M. Klene, J. E. Knox, J. B. Cross, V. Bakken, C. Adamo, J. Jaramillo, R. Gomperts, R. E. Stratmann, O. Yazyev, A. J. Austin, R. Cammi, C. Pomelli, J. W. Ochterski, R. L. Martin, K. Morokuma, V. G. Zakrzewski, G. A. Voth, P. Salvador, J. J. Dannenberg, S. Dapprich, A. D. Daniels, O. Farkas, J. B. Foresman, J. V. Ortiz, J. Cioslowski and D. J. Fox, *GAUSSIAN 09 (Revision C.1)*, Gaussian, Inc., Wallingford, CT, 2010.

63. Y. F. Liu, J. X. Ding, R. Q. Liu, D. H. Shi and J. F. Sun, *J. Photochem. Photobiol. A*, 2009, **201**, 203-207.

64. P. Verma and H. Pal, *J. Phys. Chem. A*, 2012, **116**, 4473-4486.

65. A. Trifonov, I. Buchvarov, H. A. Wagenknecht and T. Fiebig, *Chem. Phys. Lett.*, 2005, **409**, 277-280.

66. T. Yanai, D. P. Tew and N. C. Handy, *Chem. Phys. Lett.*, 2004, **393**, 51-57.

67. M. Pecul and K. Ruud, *Phys. Chem. Chem. Phys.*, 2011, **13**, 643-650.

Figure Captions

Figure 1. Molecular structures of (A) C500 and (B) Diox.

Figure 2. Three positions to form hydrogen bonds in C500.

Figure 3. Normalized steady-state absorption and fluorescence spectra of C500 in (A) Diox and (B) MeOH solvents. $\lambda_{\text{ex}} = 400$ nm. $c = 50 \mu\text{M}$.

Figure 4. Transient absorption spectra of C500 in (A) Diox and (B) MeOH solvents, registered at different time delays after excitation. $\lambda_{\text{ex}} = 400$ nm. $c = 50 \mu\text{M}$.

Figure 5. Kinetics of transient absorption for C500 in (A) Diox and (B) MeOH solvents at 426 nm, 480 nm. Solid lines correspond to results of the least-squares fitting.

Figure 6. 3D Image plot of transient absorption for C500 in (A) Diox and (B) MeOH solvents as a function of wavelength and time delay after excitation.

Figure 7. Optimized geometric structures of hydrogen-bonded complexes C500-Diox and C500-(MeOH)₃ in the ground state. (A) Top view; (B) Side view.

Figure 8. Frontier molecular orbitals (MOs) of hydrogen-bonded complexes C500-Diox and C500-(MeOH)₃.

Figure 9. The twisting of 7-NHEt group in C500-(MeOH)₃ from ICT to TICT state.

Figure 10. Different ultrafast excited state deactivation schemes for C500 in (A) Diox and (B) MeOH solvents.

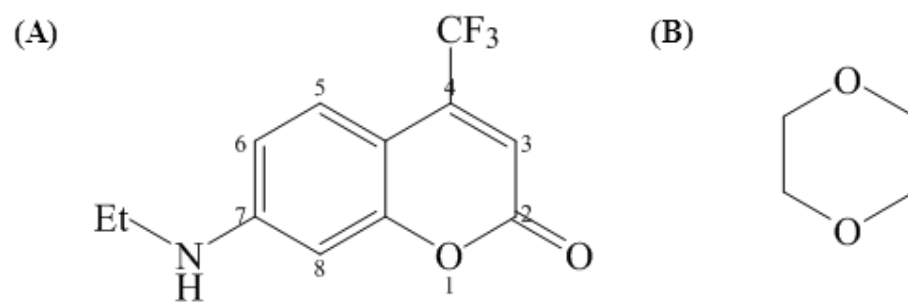


Figure 1

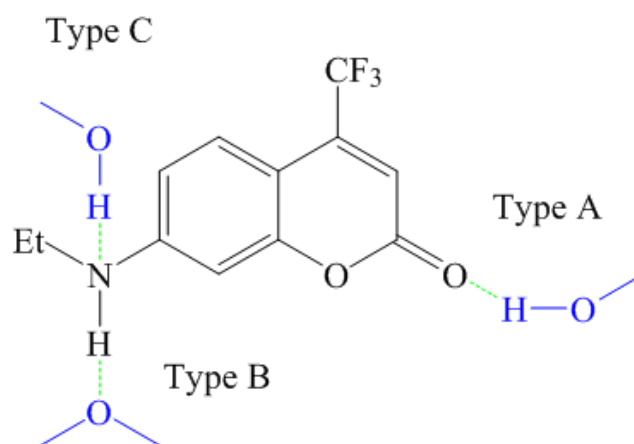
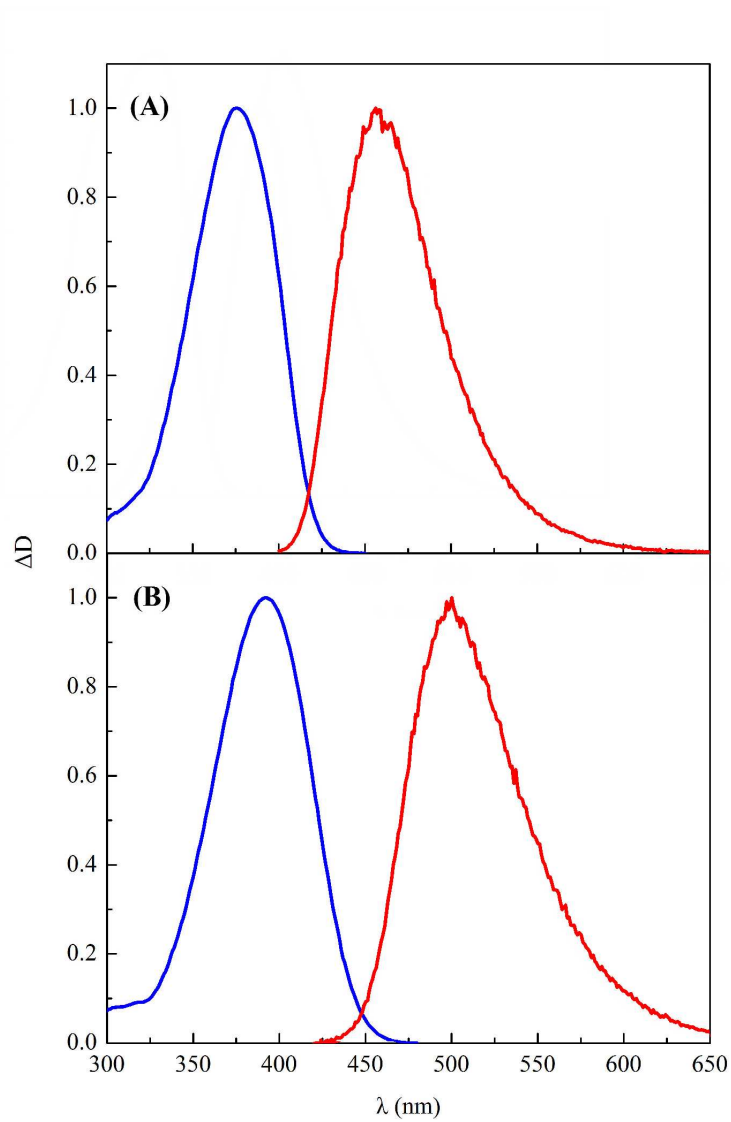


Figure 2

**Figure 3**

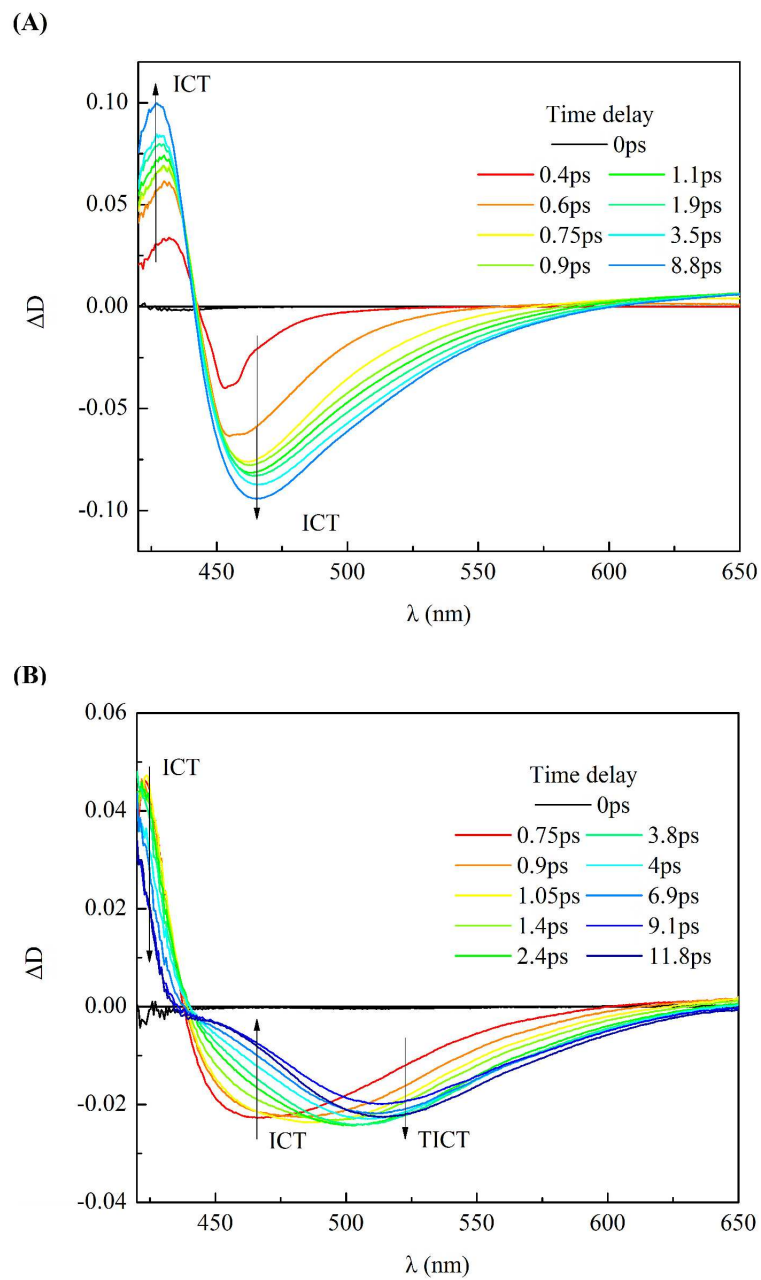
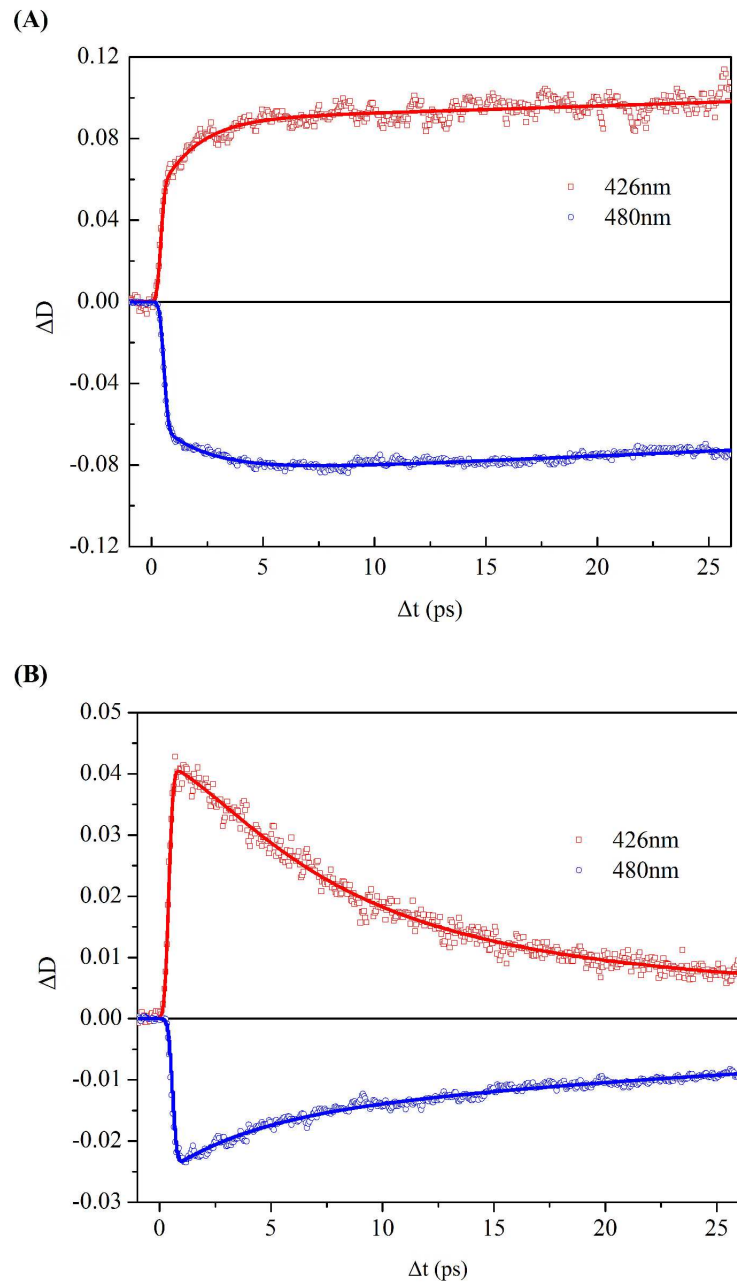


Figure 4

**Figure 5**

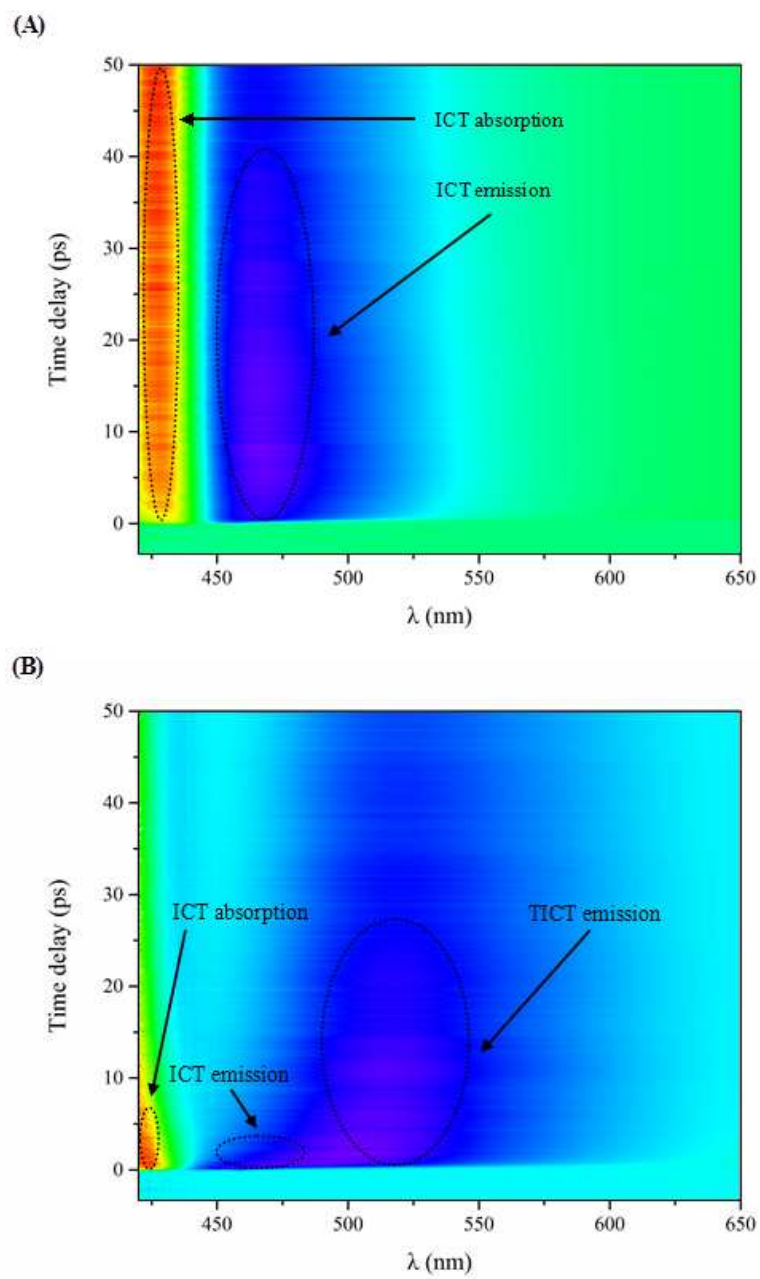


Figure 6

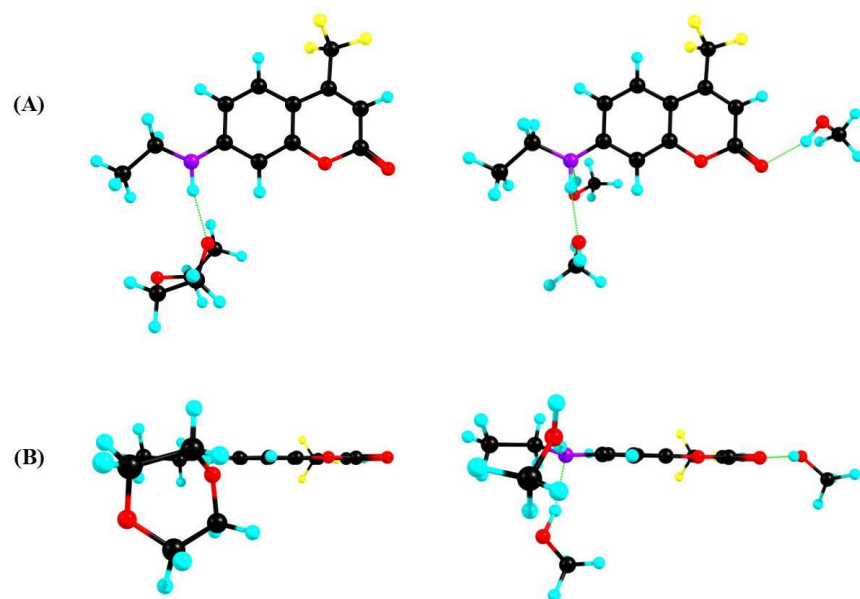


Figure 7

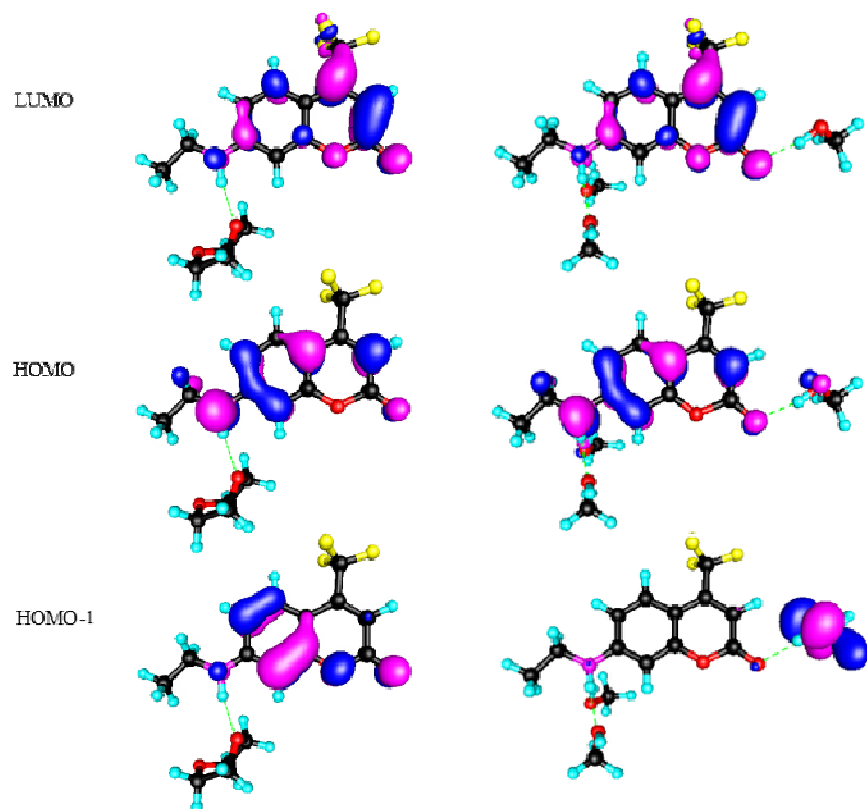


Figure 8

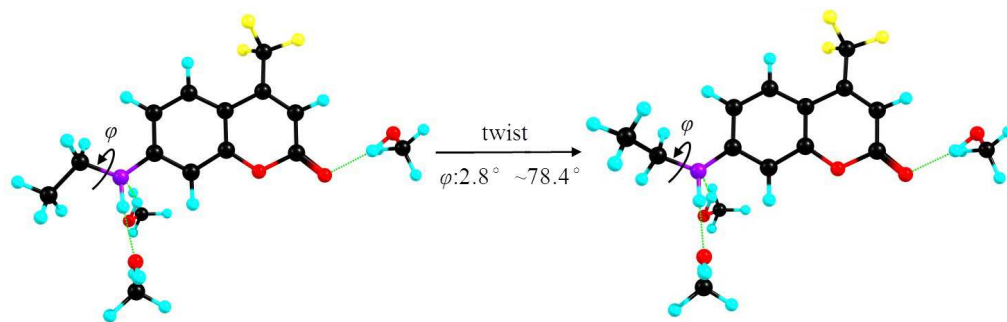


Figure 9

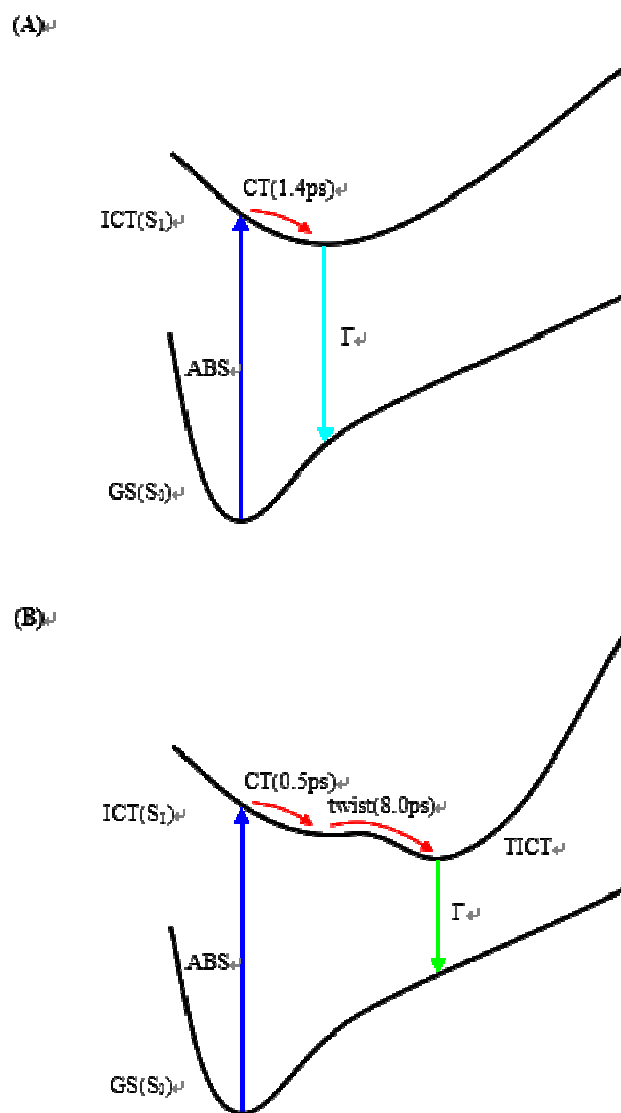


Figure 10

Table 1 Calculated electronic excitation energies (nm), the corresponding oscillation strengths and FMOs for hydrogen-bonded complexes C500-Diox and C500-(MeOH)₃ in low-lying electronically excited states by BP86(RI) and CAM-B3LYP.

Functional	C500-Diox		C500-(MeOH) ₃	
	BP86(RI)		BP86(RI)	CAM-B3LYP
S ₁	427(0.220)		511 (0.000)	309 (0.501) ^b
	H→L 87.4%		H-1→L 96.1%	H→L 68.7% ^b
S ₂	350 (0.000)		420 (0.227)	264 (0.001) ^b
			H→L 84.2%	H-1→L 56% ^b
S ₃	347 (0.080)		405 (0.000)	
S ₄	339 (0.000)		344 (0.080)	
S ₅	313 (0.000)		336 (0.000)	
S ₆	298 (0.022)		313 (0.001)	
S ₇	274 (0.110)		312 (0.000)	
S ₈	270 (0.000)		292 (0.001)	
S ₉	253 (0.115)		290 (0.023)	

Table 2 Transient absorption kinetics lifetimes of C500 in Diox and MeOH solvents by global analysis.

Solute	Solvent	τ_1 (ps)	τ_2 (ps)
C500	Diox	1.415±0.2099(14.8%)	—
	MeOH	0.4956±0.1105(22.3%)	8.065±0.8228(10.2%)

Table 3 Calculated lengths (\AA) of intermolecular hydrogen bonds in the ground state and ICT state for complexes C500-Diox and C500-(MeOH)₃.

Type of HB	C500-Diox		C500-(MeOH) ₃	
	Type B	Type A	Type B	Type C
GS	1.999	1.905	1.930	2.028
ICT	1.902	1.852	1.848	2.404
ICT minus GS	-0.097	-0.053	-0.082	0.376